

Topological properties of Sb(111) surface: A density functional theory study

Shuang-Xi Wang,^{1,2,3} Ping Zhang,^{3,*} and Shu-Shen Li¹

¹*State Key Laboratory for Superlattices and Microstructures,
Institute of Semiconductors, Chinese Academy of Sciences,
P. O. Box 912, Beijing 100083, People's Republic of China*

²*Department of Physics, Tsinghua University, Beijing 100084, People's Republic of China*

³*LCP, Institute of Applied Physics and Computational Mathematics,
P.O. Box 8009, Beijing 100088, People's Republic of China*

(Dated: October 29, 2018)

By using first-principles plane wave calculations, we systematically study the electronic properties of the thin film of antimony in (111) orientation. Considering the spin-orbit interaction, for stoichiometric surface, the topological states keep robust for six bilayers, and can be recovered in the three bilayer film, which are guaranteed by time-reversal symmetry and inverse symmetry. For reduced surface doped by Bi or Mn atom, localized 3-fold symmetric features can be identified. Moreover, the non-trivial topological states stand for non-magnetic substituted Bi atom, while can be eliminated by adsorbed or substituted magnetic Mn atom.

PACS numbers: 68.55.Ln, 71.70.Ej, 73.20.At

I. INTRODUCTION

A new state of quantum matter-topological insulator (TI)-has recently attracted great interest in condensed matter physics^{1,2}. The realization of TI HgTe both from theoretical prediction and experimental observation^{3,4}, open up opportunities for its potential application in semiconductor spintronics. It is believed that the quantum spin Hall effect as well as the time-reversal symmetry plays an important role in the new material, protecting the system from being disturbed by small perturbation caused by defects. This urges people to desire for more other promising materials, such as the Bi-based alloy $\text{Bi}_{1-x}\text{Sb}_x$, and layered compound Bi_2X_3 ($\text{X}=\text{Se}, \text{Te}$)⁵⁻⁸. Recently, the semimetallic antimony has been drawing lots of attention by its novel topological properties, and has become the proto-type system of TI⁹⁻¹².

Distinct from Bi, which is topologically trivial, according to the parity of the band at the Γ point¹³, Sb has been identified to be a strong TI¹⁴. Experimentally, it has been pointed out that the spin-split surface bands of Sb within its bulk band gap are connected to the conduction band and valence band^{9,10}. Moreover, the topologically nontrivial Sb thin films exhibit novel properties and provide a promising basis for spintronics applications such as device design and integration¹².

Nevertheless, it is apparent that the detailed analysis of the electronic structures of Sb is lacking, and there are still many unanswered questions. Especially for the Sb(111) surface, it is much desirable to identify the layer-dependence of the topological states of Sb thin film, and the modulating of the surface properties by impurities with or without magnetic moment^{15,16}. Therefore, it is instructive to investigate the electronic structures of Sb to deeply understand its topological properties. This is not only of fundamental conceptual interest for understanding the properties of TIs, but also paves the way for realizing promising application of the new state of

matter.

In this paper, we systematically study the properties of Sb(111) surface by means of first-principles calculations. The bulk band structure of Sb is presented to reveal the domination of spin-orbit interaction (SOI) for topological properties of Sb. For the stoichiometric Sb(111) surface, we investigate the layer-dependence of the surface states of Sb thin film. Moreover, we calculate the surface properties of Sb when impurities are introduced, including substituted nonmagnetic Bi and magnetic Mn, as well as the adsorbed Mn, and interesting results are obtained.

The rest of the paper is organized as follows. In Sec. II the computational methods are briefly described. In Sec. III we present and discuss our results for the bulk and surface properties of Sb. Finally, in Sec. IV, we close our paper with conclusions of our main results.

II. COMPUTATIONAL METHODS

The calculations are performed within density functional theory using the Vienna *ab-initio* simulation package (VASP)¹⁷. The PBE¹⁸ generalized gradient approximation and the projector-augmented wave potential¹⁹ are employed to describe the exchange-correlation energy and the electron-ion interaction, respectively. Here the Sb 5s and 5p electrons are treated as valence electrons. The SOI that has been confirmed to play an important role in the electronic structure of TI, is included during the calculation. The cutoff energy for the plane wave expansion is set to 400 eV. And a Fermi broadening²⁰ of 0.1 eV is chosen to smear the occupation of the bands around the Fermi level by a finite- T Fermi function and extrapolating to $T = 0$ K.

The Sb(111) surface is modeled by a slab composing of several(1-6) bilayers (BL), and a vacuum region of 20 Å. Obviously, existence of the surface breaks the equivalence of the Sb atomic positions in a layer, hence through-

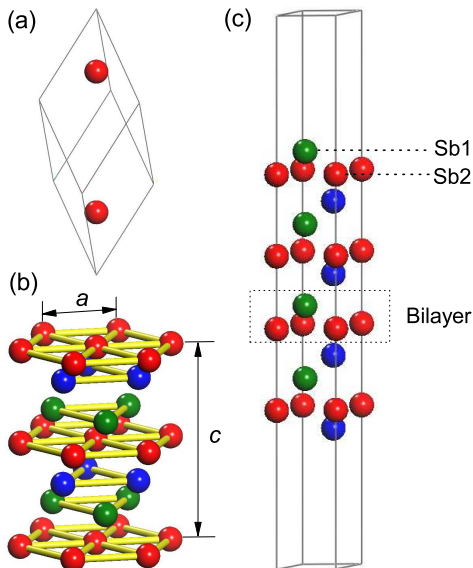


FIG. 1: (Color online) Atomic structure of bulk Sb and Sb(111) surface. (a) Primitive cell of bulk Sb, (b) hexagonal unit cell of bulk Sb, (c) slab model of Sb(111) surface.

out this paper, we employ the notation Sb1 for the first atomic plane, and Sb2 for the second atomic plane from the surface, which are shown in Fig. 1(c). Integration over the Brillouin zone is done using the Monkhorst-Pack scheme²¹ with $21 \times 21 \times 1$ grid points for the $p(1 \times 1)$ surface; for the $p(3 \times 3)$ surface, $7 \times 7 \times 1$ grid points are used. The structures of slab are fully optimized until the maximum residual ionic force is below $0.02 \text{ eV}/\text{\AA}$.

III. RESULTS AND DISCUSSION

The crystal structure of Sb is rhombohedral with the space group $D_{3d}^5(R\bar{3}m)$, with two bismuth atoms in the trigonal unit cell (see Fig. 1(a)). Equivalently, it can be represented in terms of a hexagonally arranged layer structure, which is shown in Fig. 1(b). The hexagonal unit cell has three sets of bilayers, where each bilayer consists of two Sb atoms. Structurally, bilayers in Sb form a stable unit with strong intrabilayer bonds, while the interbilayer bonding is much weaker. The calculated structure parameters are $a = 4.392 \text{ \AA}$, $c = 11.432 \text{ \AA}$, which are close to experimental data $a = 4.3007 \text{ \AA}$, $c = 11.222 \text{ \AA}$ ²². Moreover, the optimized internal parameter is 0.233, consistent well with the experimental measurement 0.234.

It has been proposed that Sb is a strong TI by calculating its Z_2 invariant ν ($=1$) from the knowledge of the parity of the occupied Bloch wave function at the time-reversal invariant Γ point in the Brillouin zone¹⁴. This means that the SOI dominates the electronic nature of Sb, which can be seen from the band structure (see Fig. 2). It is clear that the band gap is very small without

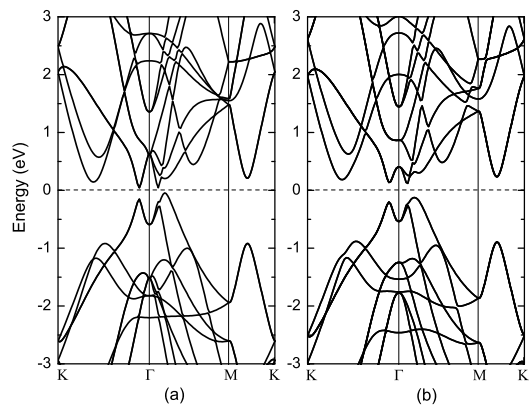


FIG. 2: Bulk band structure without SOI (a) and with SOI (b). The Fermi level is set to zero.

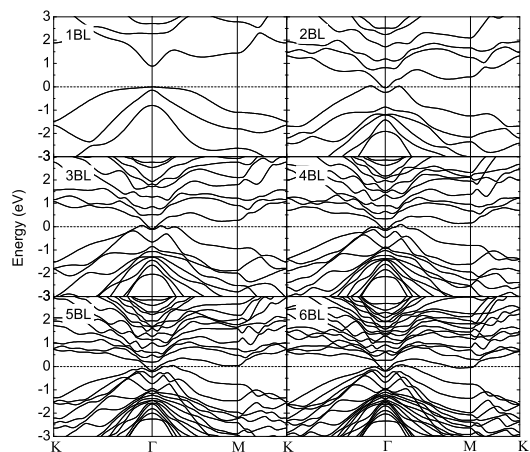


FIG. 3: Surface band structure with one to six bilayer thickness. The Fermi level is set to zero.

SOI. While as the SOI is taken into consideration, the band gap is enlarged up to about 0.237 eV . Moreover, because of its topological electronic nature, we can expect the existence of gapless surface states. Therefore, in the following we will focus our attention on the properties of Sb(111) surface.

It is well known that the topological features are of strongly thickness dependence of the TI thin film. For thinner film, the coupling between top and bottom surfaces is strong enough to open up a whole insulating gap. While with increasing thickness, the inter-surface coupling becomes weaker and the topological features will be recovered. This is the same case for Sb(111) surface. As illustrated in Fig. 3, we show the evolution of band structure of Sb films with the thickness from the single BL to six BL. In a single BL film, the Sb electronic states (mainly from $5p$ orbital) split into two parts forming a gap around the Fermi level. The gap is as large as about 0.9 eV , implying the strong coupling between two surfaces. In the case of two BL film, the splitting of

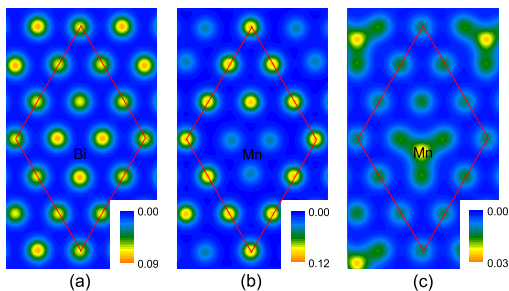


FIG. 4: (Color online) Surface charge density distributions at the height of 2.0 Å above the reduced Sb(111) surface: (a) Bi-substituted, (b) Mn-substituted and (c) Mn-adsorbed.

$5p$ states decrease with the decline of the coupling, leading to a semimetallic electronic structure. Obviously, the topological features start to appear in the three BL case, where a non-trivial helical edge state ($\nu_0=1$) below the Fermi level at Γ point can be identified. This helical state is consist of two surface states degenerated at Γ point but separated in energy elsewhere by SOI¹². Nevertheless, it is noticeable that for the case of four BL and five BL films, the gaps are opened up again at Γ point. This can be attributed to the inverse asymmetry of the films with four and five BL. While the topological states should be recovered when the number of BL of the film is multiples of three, which conserves the inverse symmetry. As expected, it can be seen that the topological states are recovered for six BL. The double degenerate Sb(111) surface states contain a single Dirac cone at the Γ point, which is robust and topologically protected by time-reversal symmetry. The Dirac point is about 160 meV below the Fermi level, within the bulk band gap. Compared with the experimental value of 230 meV¹¹, the difference may arise from the subsurface defects observed in the experiment.

Various impurities (magnetic or not) may have different impact on the degeneracy and topological properties of Sb energy bands, which will be illustrated in the following discussions based on the six BL film. It has been shown that the alloy $\text{Bi}_{1-x}\text{Sb}_x$ is a 3D TI^{14,23,24}. Here it would be interesting to investigate the surface state properties of reduced Sb(111) surface with the existence of Bi as a nonmagnetic impurity. Moreover, as a comparison, a magnetic impurity (Mn atom) is also taken into consideration. During the calculations, the $p(3\times 3)$ surface is adopted with the substituted impurities Bi or Mn atom taking the position of one subsurface Sb2 atom on each surface, while the adsorbed Mn atoms are symmetrically located at the stable hcp sites above two surfaces of Sb(111).

Figure 4 presents the surface charge density distributions as simulation of STM topography at the height of 2.0 Å above the Bi-substituted, Mn-substituted and Mn-adsorbed surface, respectively. One can see clearly that the localized 3-fold symmetric features can be identified

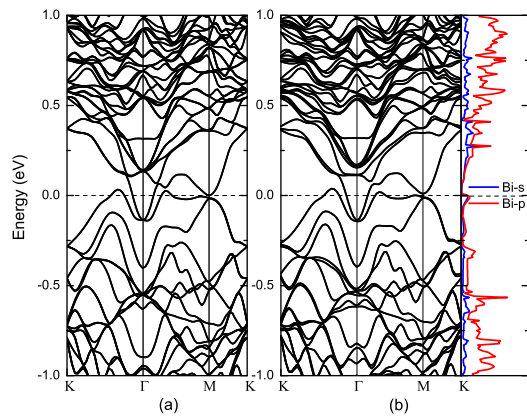


FIG. 5: (Color online) The band structure of clean (a) and Bi substituted (b) Sb(111) surface.

from all of three surfaces, especially for the Mn-doped ones. For the Bi-substituted surface, only tiny difference exists between the region above the Bi atom and others, and this can be attributed to that Bi and Sb belong to the same chemical group and possess the same number of valence electrons. As a result the Bi-doped Sb(111) surface may maintain the topological features, which will be illustrated later by its band structure. For the Mn-doped surfaces, however, more evident different features can be observed. It is noticeable that the charge distribution is strongly depleted at the position just above the substituted Mn atom, while the adsorbed Mn atom can be identified clearly by the charge accumulation. Keeping in mind that the magnetism of Mn atom, we will see that the magnetic impurity can have significant effect on the surface states of Sb(111) surface.

The band structure of Bi-doped Sb(111) surface is presented in Fig. 5(b). For comparison, the band structure of stoichiometric $p(3\times 3)$ Sb(111) surface is also shown in Fig. 5(a). It is clear that the topological surface state remains to be robust despite of the existence of Bi impurity, and the Dirac point of this reduced surface almost stays at the same position as that of the stoichiometric surface. This can be attributed to the following reasons. (i) The time-reversal symmetry stands against nonmagnetic impurities. (ii) The energy bands of Bi-doped system remain degenerate thus keep gapless. Moreover, from the PDOS of Bi we can see that the doped Bi atom contributes little to the band structure near the Fermi level and the Dirac point, thus the topological features of Sb keep robust, which also consists with the fact that the alloy $\text{Bi}_{1-x}\text{Sb}_x$ is a 3D TI inherited from Sb¹⁴.

Theoretically, if the impurity carries a magnetic moment, the time-reversal symmetry is explicitly broken, and a local energy gap will be opened up at the Dirac point¹⁶. While up to now relevant experimental observations are lack yet, therefore it is desirable to have a direct and intuitional sight into it. By calculations we find that the magnetic impurities can obviously lift the degener-

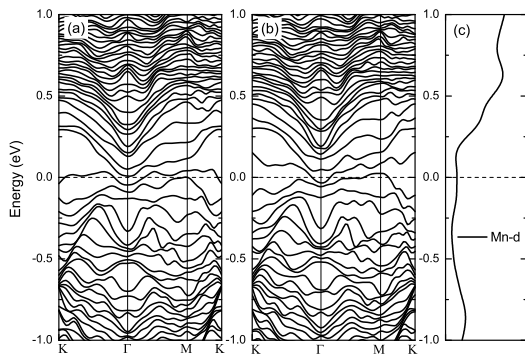


FIG. 6: The band structure of Mn-substituted Sb(111) surface: (a) spin-up, (b) spin-down and (c) the PDOS of the Mn atomic d -bands.

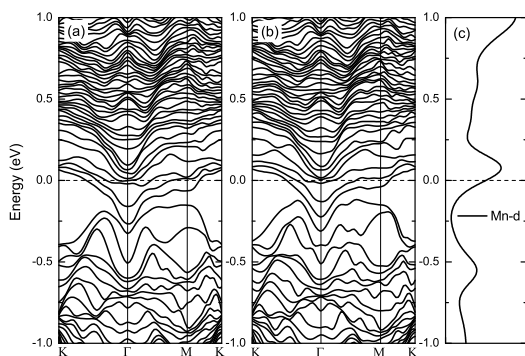


FIG. 7: The band structure of Mn-adsorbed Sb(111) surface: (a) spin-up, (b) spin-down and (c) the PDOS of the Mn atomic d -bands.

acy protected by the time-reversal symmetry. For clarity, here we plot the lifted band structures of Mn-substituted and adsorbed Sb(111) surfaces dividedly in (a) and (b) of Fig. 6 and Fig. 7, labeled by spin-up and spin-down, respectively. It can be seen that both of the magnetic impurities eliminate the Dirac point by opening up a gap at Γ point. From the PDOS (See Fig. 6(c) and Fig. 7(c)), we find that unlike the doped Bi atom, the magnetic d orbital of Mn atom contributes much to the states near the Dirac point, hence clearly breaks the time-reversal symmetry. As expected¹⁶ a ferromagnetic ground state is formed on the TI surface by the introduced magnetic Mn impurity.

IV. CONCLUSIONS

In conclusion, we have systematically studied the topological properties of Sb(111) surface by density functional calculation. We found that the stoichiometric Sb(111) surface possesses single Dirac point protected by the time-reversal symmetry and inverse symmetry. And the topological states are layer dependent and keep robust for six bilayers film. Moreover, we revealed that the non-trivial topological states stand for non-magnetic substituted Bi, while the substituted or adsorbed magnetic Mn atom can obviously eliminate the Dirac point. We expect the present results for the topological features of Sb are greatly helpful for understanding and application of the topological insulator.

* Corresponding author; zhang_ping@iapcm.ac.cn

¹ M. Z. Hasan and C. L. Kane, *Rev. Mod. Phys.* **82**, 3045 (2010).

² X.-L. Qi and S.-C. Zhang, arXiv:1008.2026v1 [*Rev. Mod. Phys.* (to be published)].

³ B. A. Bernevig, T. L. Hughes, and S. C. Zhang, *Science* **314**, 1757 (2006).

⁴ M. König, S. Wiedmann, C. Brüne, A. Roth, H. Buhmann, L. W. Molenkamp, X. L. Qi, and S. C. Zhang, *Science* **318**, 766 (2007).

⁵ Y. Xia, D. Qian, D. Hsieh, L. Wray, A. Pal, H. Lin, A. Bansil, D. Grauer, Y. S. Hor, R. J. Cava, and M. Z. Hasan, *Nature Phys.* **5**, 398 (2009).

⁶ H. Zhang, C. X. Liu, X. L. Qi, X. Dai, Z. Fang, and S. C. Zhang, *Nat. Phys.* **5**, 438 (2009).

⁷ Y. L. Chen, J. G. Analytis, J.-H. Chu, Z. K. Liu, S.-K. Mo, X.-L. Qi, H. J. Zhang, D. H. Lu, X. Dai, Z. Fang, S. C. Zhang, I. R. Fisher, Z. Hussain, and Z.-X. Shen, *Science* **325**, 178 (2009).

⁸ T. Zhang, P. Cheng, X. Chen, J.-F. Jia, X. Ma, K. He, L. Wang, H. Zhang, X. Dai, Z. Fang, X. Xie, and Q.-K. Xue, *Phys. Rev. Lett.* **103**, 266803 (2009).

⁹ K. Sugawara, T. Sato, S. Souma, T. Takahashi, M. Arai,

and T. Sasaki, *Phys. Rev. Lett.* **96**, 046411 (2006).

¹⁰ D. Hsieh, Y. Xia, L. Wray, D. Qian, A. Pal, J. H. Dil, J. Osterwalder, F. Meier, G. Bihlmayer, C. L. Kane, Y. S. Hor, R. J. Cava, and M. Z. Hasan, *Science* **323**, 919 (2009).

¹¹ K. K. Gomes, W. Ko, W. Mar, Y. Chen, Z.-X. Shen, and H. C. Manoharan, arXiv:1008.2026v1.

¹² G. Bian, T. Miller, and T.-C. Chiang, *Phys. Rev. Lett.* **107**, 036802 (2011).

¹³ Y. Liu and R. E. Allen, *Phys. Rev. B* **52**, 1566 (1995).

¹⁴ L. Fu and C. L. Kane, *Phys. Rev. B* **76**, 045302 (2007).

¹⁵ X.-L. Qi, T. L. Hughes, and S.-C. Zhang, *Phys. Rev. B* **78**, 195424 (2008).

¹⁶ Q. Liu, C.-X. Liu, C. Xu, X.-L. Qi, and S.-C. Zhang, *Phys. Rev. Lett.* **102**, 156603 (2009).

¹⁷ G. Kresse and J. Furthmüller, *Phys. Rev. B* **54**, 11169 (1996) and references therein.

¹⁸ J. P. Perdew, K. Burke, and M. Ernzerhof, *Phys. Rev. Lett.* **77**, 3865 (1996).

¹⁹ G. Kresse and D. Joubert, *Phys. Rev. B* **59**, 1758 (1999).

²⁰ M. Weinert and J. W. Davenport, *Phys. Rev. B* **45**, 13709 (1992).

²¹ H. J. Monkhorst and J. D. Pack, *Phys. Rev. B* **13**, 5188

- (1976).
- ²² C. S. Barrett, P. Cucka, and K. Haefner, *Acta. Cryst.* **16**, 451 (1963).
- ²³ D. Hsieh, D. Qian, L. Wray, Y. Xia, Y. S. Hor, R. J. Cava, and M. Z. Hasan, *Nature* **452**, 970 (2008).
- ²⁴ Jeffrey C. Y. Teo, Liang Fu, and C. L. Kane, *Phys. Rev. B* **78**, 045426 (2008).
- ²⁵ Yu. M. Koroteev, G. Bihlmayer, E. V. Chulkov, and S. Blügel, *Phys. Rev. B* **77**, 045428 (2008).